### 3.1.6 Additional Research

#### 3.1.6.1 Define Attrition Resistance

The powder sample of RJO-181 (30 wt.% $Fe_2O_3/SiO_2$) was used for microhardness test. Cold molds using epoxy hardeners were used to prepare the specimens. After imbedding the particles in the epoxy, they were allowed to harden. Then the epoxy molds were polished. Several particles were photographed in the optical microscope. Using a MICROMET-4 hardness tester, the microhardness measurements were made. The specimen was mounted onto the hardness tester, and a load of 25 gm was used to make the Vicker's indentation on the particles, which are 10 to 50 microns in size. The indentations were so large that they covered the entire particles. Hence, a load of 10 gm (the minimum load available) was used to make the indentations on several individual particles embedded in the epoxy mold. After making the indentations the specimen was mounted on the optical microscope and the diagonal distances of the indentations were measured. The average value of about 50 indentations was taken for measuring the Vicker's hardness, which was calculated to be 40 $kg/mm^2$. According to the ASTM standards, this number indicates that the material under investigation is very soft. The value of 40 is not accurate, as the hard epoxy under the particles can also take part of the load. This introduces additional uncertainty to the calculated value. For comparison, the hardness values for several materials are plotted in Figure 1. It can therefore be concluded that the iron oxide catalyst particles are very soft.

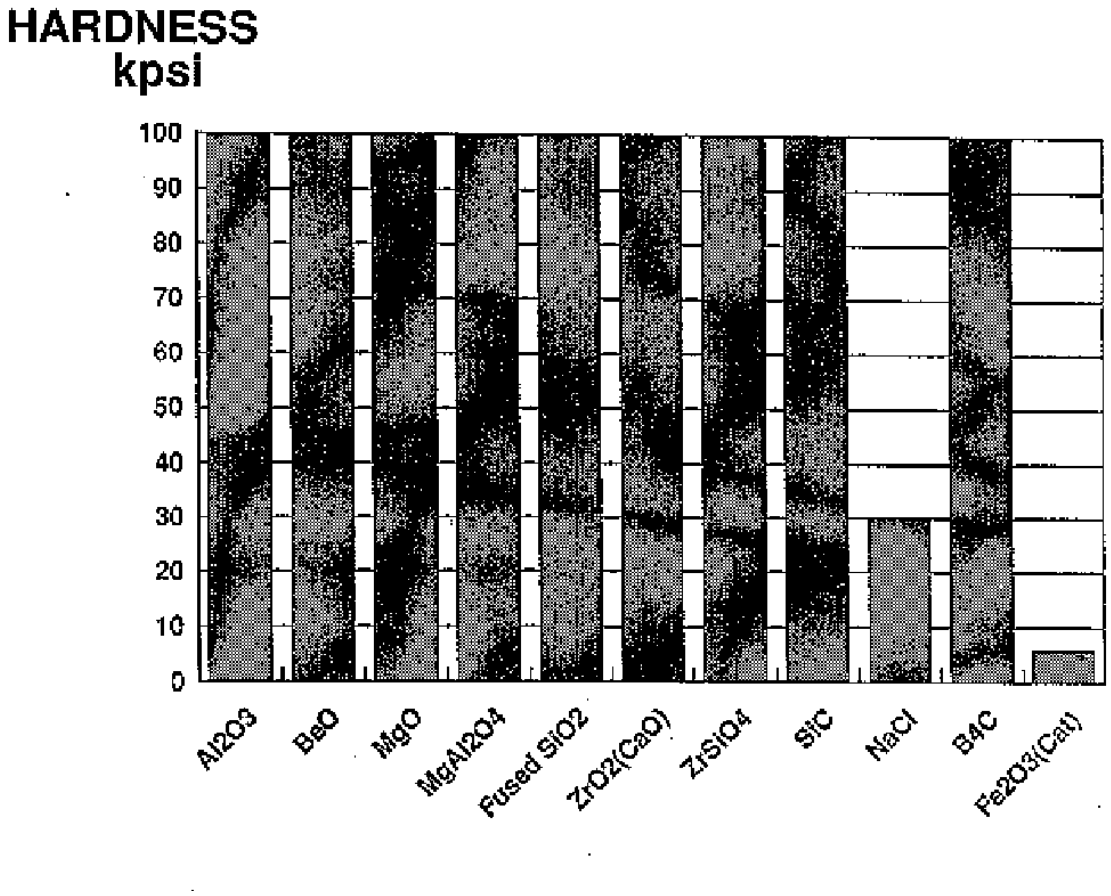


Figure 1. A comparison of the hardness of a $Fe_2O_3/SiO_2$ catalyst to other materials.

### 3.1.6.2 Effect of Carbon Deposition

Iron catalysts that have high FTS activity contain bulk iron carbide and large amounts of excess carbon. Pretreatment of the 100Fe/3.6Si/0.71K catalyst with CO at 270°C and 13 atm for 24 hr yields a highly active catalyst and yet produces about twice as much carbon as needed for the formation of $Fe_5C_2$. It is of interest to determine the role of this carbon in the FTS and determine its morphology.

The 100Fe/3.6Si/0.71K catalyst was subjected to syngas ($H_2$/CO=0.7) activation at 270°C and 13 atm. After 93 hr of synthesis, during which the CO conversion never rose above 12%, $H_2$ flow was stopped and the catalyst was treated with CO for 22 h. Following the CO treatment the synthesis was restarted. As can be seen in Figure 1, the CO conversion rose very rapidly and reached the same level as when the catalyst is initially activated with CO. X-ray diffraction analysis of catalyst samples withdrawn before and after treating the catalyst with CO show that syngas activation converted the catalyst to $Fe_3O_4$ and the CO treatment partially reduced the $Fe_3O_4$ to $\chi$-$Fe_5C_2$ and $\epsilon'$-$Fe_{2.2}C$. Mössbauer spectroscopy results showing the phase transformation is shown in Figure 2. Catalyst samples from this run were submitted to Sandia for high-resolution TEM analysis. High resolution TEM of this catalyst series offers the possibility of showing the location of the iron carbide in relation to the $Fe_3O_4$ and the structure of the free carbon which forms from CO activation.

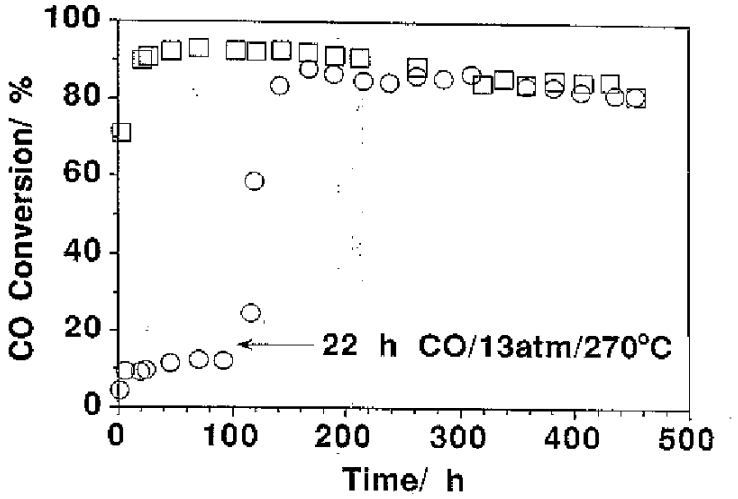


Figure 1. Comparison of the CO conversion vs. Time-on-stream for the 100Fe/3.6Si/0.71K catalyst. □- activated with CO at 270°C, 13 atm for 24 hr and ○- activated with $H_2/CO = 0.7$ at 270°C and 13 atm followed by a 22 hr treatment with CO at 270°C and 13 atm. Synthesis conditions: $H_2/CO = 0.7$ at 13 atm and 270°C.

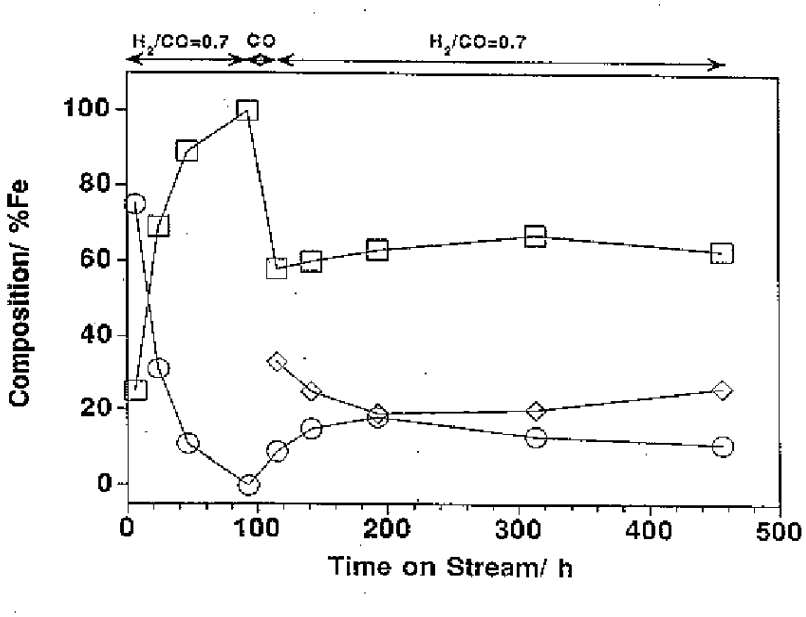


Figure 2. Mössbauer spectroscopy results for the 100Fe/3.6Si/0.71K catalyst activated with $H_2/CO = 0.7$ at 270°C and 13 atm followed by a 22 hr treatment with CO at 270°C and 13 atm. Synthesis conditions: $H_2/CO = 0.7$ at 13 atm and 270°C. ○- superparamagnetic phase, □- $Fe_3O_4$ and ◇- iron carbide.

## 3.2.0 Task 3. Catalyst Structure and Characterization

### 3.2.1 Fischer-Tropsch Iron Catalysts: Characterization by Electron Microscopy

### INTRODUCTION

The Fischer-Tropsch conversion process for producing hydrocarbons from synthesis gas using iron oxide catalysts is well known.[1] In this process synthesis gas (mixture of CO and $H_2$) is converted over various catalysts to yield a range of hydrocarbon products, which may be refined into synthetic fuels. Catalysts such as iron, cobalt, ruthenium and nickel in their oxide forms, are commonly used for this FT process. Different catalysts yield different product distributions under similar reaction conditions. Schultz *et al.*[2] hypothesized that $Fe_3O_4$ (magnetite form) has no synthesis activity and the degree of oxidation of iron to magnetite has limitations on the maximum activity of the catalyst. However, Dwyer *et al.*[3] showed that higher yields could be obtained over the preoxidized iron foils than the reduced iron foils.

When the iron oxide catalysts are used for the Fischer-Tropsch synthesis, several forms of iron oxides and iron carbides are formed.[4-7]. These include iron oxides (hematite and magnetite) and iron carbides, which are known to exist in five or six different forms, namely, $\epsilon$-$Fe_2C$, $\epsilon'$-$Fe_{2.2}C$, $\chi$-$Fe_{2.5}C$, $Fe_3C$, FeC, $Fe_7C_3$, etc. The fact that how these phases are formed and at what stage of the reaction pathway, is still subject to debate. Both the formation of these phases during reaction conditions, and their relationship to the activity/selectivity of the catalysts are interesting phenomena. In this investigation, we have attempted to determine the phases formed in a typical iron oxide catalyst prepared in-house through a precipitation process, using X-ray diffraction and high resolution electron microscopy.

## EXPERIMENTAL

Iron oxide catalysts were prepared by a precipitation process containing 4.4 wt.% $SiO_2$ and 3.6% $K_2O$ (balance $Fe_2O_3$). $SiO_2$ and $K_2O$ were added as promoters. This catalyst was subjected to Fischer-Tropsch synthesis in a slurry phase reactor, and the samples were withdrawn at different time intervals.

An appropriate amount of catalyst was mixed with $C_3$ oil to obtain a 10% slurry in a slurry phase reactor. Then this slurry was pretreated in flowing carbon monoxide at 270$^{o}$C for about 27 hours at atmospheric pressure in order to activate the catalyst. After activation, a portion of the slurry sample was withdrawn from the reactor through a dip-tube. Catalyst sample was separated from the slurry (oil) by Soxhlet extraction using THF.

After this step, the pressure in the reactor was raised to 75 psig and the passage of synthesis gases was returned to carry out the reaction in the slurry phase. While the reaction was in progress, product gases were analyzed to estimate the conversion levels with time.

Catalyst samples in slurry were withdrawn at regular intervals with the dip-tube. The samples thus withdrawn were imbedded in wax. Catalyst particles were separated from the wax using o-xylene as solvent in a Soxhlet extraction unit. The catalyst separated and cleaned from the wax was then used for characterization studies.

Transmission Electron Microscopy

Several samples were selected for electron microscopy work. For this, a Hitachi HF2000, equipped with a field emission gun, analytical electron microscope was used. The operating voltage was 200 kV. The field emission gun employs a single crystal emitter with a very fine point that generates a beam with 100-1000 times the brightness

of the standard thermionic emitter with a much finer ultimate diameter. The field emission electron beam has a much lower energy spread (i.e., higher coherency) than the thermionic emitter beam, thus allowing us to obtain improved high resolution imaging. The microscope has an image resolution of 0.24 nm point-to-point in a standard imaging mode. The microscope was also equipped with a windowless X-ray detector (PGT) thus allowing us to obtain X-ray analysis from regions as small as 1 nm in diameter.

Also, a JEOL 4000EX, a high resolution electron microscope was used at 400 kV. The 0.17 nm point-to-point resolution of this microscope allows us to obtain lattice images from the crystalline particles.

Scanning Electron Microscopy

Scanning electron microscopy was carried out at 20 kV using a Hitachi S-2700 scanning electron microscope, equipped with a $LaB_6$ filament and a thin window X-ray PGT detector for elemental analysis. All the powder samples were coated with a conductive layer of gold prior to analysis.

X-ray Diffraction

A Rigaku X-ray diffractometer was used at 40 kV, 20 mA (CuKα radiation) with a pyrolytic graphite monochromator in the diffracted beam path. Data were collected using a step width of $0.02^o$ with a count time of 5 sec/step.

**RESULTS AND DISCUSSION**

RJO-137B

The first sample analyzed was the sample just after CO pretreatment for about 27 hours and prior to the introduction of synthesis gas. This sample has a surface area of about 120 $m^2/g$ with a pore volume of 0.22 cc/g. The surface area and pore volume

data for the catalysts analyzed are given in Table 1. The X-ray diffraction showed that this sample is in $Fe_3O_4$ form. The X-ray diffraction patterns of the samples, shown in Figure 1, clearly depict all the $Fe_3O_4$ reflections. The JEPDS File #19-629 was overlaid in this figure to indicate the positions of $Fe_3O_4$ cubic reflections.

Lattice fringe images from two particles obtained from this sample are presented in Figure 2. The particle at the top shows 2.97 Å lattice fringes which correspond to $Fe_3O_4$ [220] lattice spacings. The particle at the bottom (Figure 2) depicts 4.85 Å lattice fringes corresponding to [111] planes of $Fe_3O_4$. Note that these particles do not have any surrounding films. However, the particle shown in Figure 3, has a film of about 4.2 nm width. The graphitic carbon film has a lattice spacing of ~3.4 Å, which corresponds to [002] lattices of graphitic carbon. EDS patterns using a 10 Å probe were obtained from both the surrounding film and from the center of the particle. These are shown in Figure 4. The spectra give additional evidence that the surrounding film is graphitic carbon.

RJO-137D

This sample was withdrawn from the reactor after 28 hours-on-stream. The X-ray diffraction pattern from this sample shown in Figure 1(b), indicates that this sample after 28 hours on stream mostly consists of $Fe_3O_4$. An $Fe_3O_4$ particle with a surrounding graphitic film is shown in Figure 5(a). EDS data obtained from the film showed only carbon and the data obtained from the center showed more Fe and O, and trace amounts of Al. This Al comes from both the film as well as from the center (see Figure 6), and may be an impurity. The beam damage of the specimen can be seen in Figure 5(b), where the irradiation of electron beam caused a hole of about 2.5 nm in diameter.

A typical particle with lattice fringes with its corresponding fourier transform are shown in Figure 7. The FFT can be indexed as diffraction pattern[8] and enables us to analyze the crystal structure of the particle in question. In Figure 7 the FFT obtained from an area of 256 x 256 pixels in the micrograph is in quite agreement with the diffraction pattern of $Fe_3O_4$ particle oriented in [211] direction with respect to the beam.

Several efforts made so far to get in the structural information from the fine structure of very small particles from electron diffraction patterns have indicated that there are still some difficulties.[9] For very thin specimens, Cowley[10] proved that the electron wave may be considered to travel straight through the specimen undergoing only a phase change proportional to the electrostatic potential in the specimen. The recent developments of electron optics and acquisition of images using CCD cameras make it easy to identify the fine structures of ultrafine particles[11-20]. It has been proven that the optical diffraction patterns and Fast Fourier Transform (FFT) patterns of a micrograph of atomic resolution taken under optimum conditions are equivalent to the selected area electron diffraction patterns. Even when the specimen is not very thin and dynamic scattering cannot be disregarded, the diffraction spots formed by the FFT represent the spacing of the lattice plane.[20]

RJO-137H

This sample was withdrawn after 124 hours-on-stream. The XRD pattern from this sample is presented in Figure 1(c) and exhibits all peaks corresponding to $Fe_3O_4$ (magnetite) phase. An $Fe_3O_4$ particle with a surrounding film of graphitic carbon is shown in Figure 8. In addition to this, particles of rectangular shape were observed. Typical rectangular shaped particles are presented in Figure 9. EDS pattern obtained

from one of these rectangular particles (Figure 10) exhibits Fe, Al, O. Note that the rectangular particles could not be seen for the previous samples.

RJO-137M

This sample was withdrawn from the reactor after 461 hours-on-stream. The catalyst still showed about 90% conversion of the reactants. The XRD pattern obtained from this sample is presented in Figure 1(d) and shows some iron carbide peaks. Since the strongest carbide peaks and an $Fe_3O_4$ (400) peak fall in the region of $2\theta$ = 40-46, this region is shown magnified in Figure 11. In this figure the peaks are fitted to Voigt function with the coefficient determination ($r^2$) above 0.9. In all the XRD traces given in Figure 11, the observed $Fe_3O_4$ (400) reflection is displaced from the JCPDS file, probably due to the presence of silica and potassium in the sample. The addition of silica to $Fe_3O_4$ has been found to alter the lattice parameters and this correspondingly causes a shift in $2\theta$ positions. However, in the trace of RJO-137M sample (Figure 11) the appearance of two additional peaks to the left of $Fe_3O_4$ (400) reflection corresponding to $\epsilon$'-carbide can be seen. These two peaks are evidently absent in the first three samples.

A scanning electron micrograph from this sample presented in Figure 12 indicates that this sample consists of spherical agglomerates of 30-50 $\mu$m diameter. A high resolution electron micrograph from this sample is presented in Figure 12 wherein the lattice fringes of [111], [220] and [311] planes can be seen. Several long rectangular particles were also observed which were $Fe_3O_4$ from lattice fringe measurement.

The XRD pattern for the last sample presents evidence for the presence of trace amounts of carbide. Since this carbide may be in so small a quantity, the TEM examination could not observe carbide particles.

## REFERENCES


1. Anderson, R. B. "The Fischer-Tropsch Synthesis", Academic Press, New York, 1984.
2. Schultz, J. F.; Hall, W. K.; Seligman, B.; Anderson, R. B. *J. Am. Chem. Soc.*, 1995, **77**, 213.
3. Dwyer, D. J.; Somorjai, G. A. *J. Catal.*, 1978, **52**, 291.
4. Jung, H.; Thomson, W. J. *J. Catal.*, 1992, **134**, 654.
5. Jung, H.; Thomson, W. J. *J. Catal.*, 1993, **139**, 375.
6. LeCaer, G.; Duvois, J. M.; Pijolat, M.; Perrichon, V.; Bussiere, P. *J. Phys. Chem.*, 1982, **86**, 4799.
7. Niemantsverdriet, J. W.; van der Kraan, A. M.; van Dijk, W. L.; van der Baan, H. S. *J. Phys. Chem.*, 1980, **84**, 3363.
8. Tomita, M.; Hashimoto, H.; Ikuta, H.; Endoh, T.; Yokota, T. *Ultramicrosc.*, 1985, **16**, 9.
9. Gao, P.; Gleiter, H. in "Physics and Chemistry of Small Clusters," (P. Jena, B. K. Rao, S. N Khanna, eds.) Plenum Press, NY, 1987, pp 73-78.
10. Cowley, J. M. *Acta Cryst.*, 1959, **12**, 367.
11. Allpress, J. G.; Sanders, J. V.; Wadsley, A. D. *Phys. Status Solidi*, 1968, **25**, 541.
12. Iijima, S. *J. Appl. Phys.*, 1971, **42**, 5891.
13. Iijima, S. *Acta Cryst.*, 1973, **A29**, 18.
14. Uyeda, N.; Kobayashi, T.; Suito, E.; Harada, Y.; Watanabe, M. *J. Appl. Phys.*, 1972, **46**, 1581.
15. Hashimoto, H.; Tanji, T.; Ono, A.; Kumao, A. *J. Electron Microsc.*, 1975, **24**, 212.

16. Clarke, R.; Thomas, G. *Proc. Electron Microsc. Soc. Am.*, 1976, 494.

17. Gronsky, R.; Sinclair, R.; Thomas, G. *Proc. Electron Microsc. Soc. Am.*, 1976, 492.

18. Tanji, T.; Hashimoto, H. *Acta Cryst.*, 1978, **A34**, 453.

19. Yokota, Y.; Tomita, M.; Hashimoto, H.; Endoh, H. *Ultramicroscopy*, 1981, **6**, 313.

20. Tomita, M.; Hashimoto, H.; Ikuta, T.; Endoh, H.; Yokata, Y. *Ultramicroscopy*, 1985, **16**, 9.

| Table 1 | | | |
|---|---|---|---|
| Catalyst | Pore Diameter, Å | Pore Volume, $cm^3/g$ | Surface Area ($m^2/g$) |
| RJO-137B | 140 | 0.25 | 70 |
| RJO-137D | 170 | 0.32 | 77 |
| RJO-137H | 250 | 0.48 | 77 |
| RJO-137M | 200 | 0.43 | 87 |

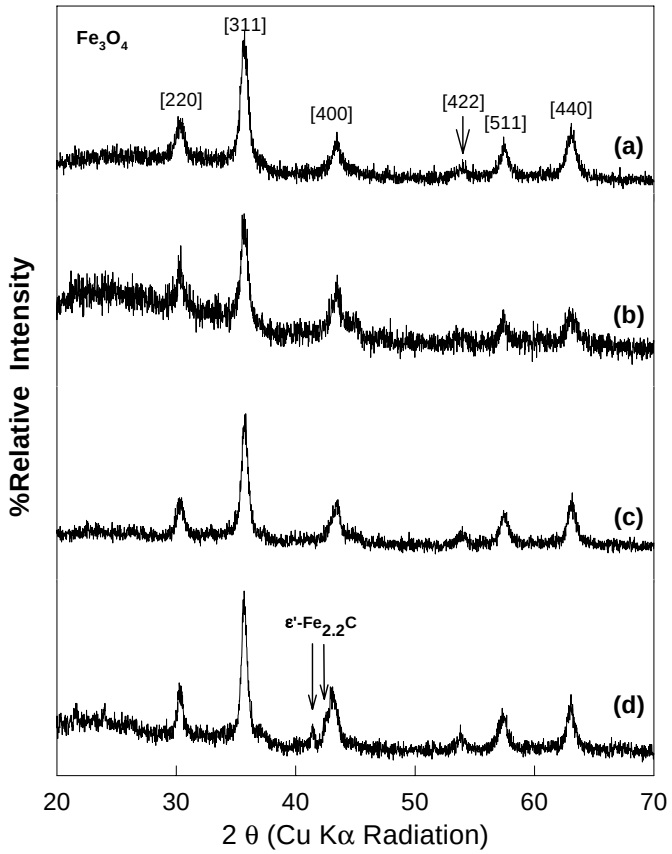


Figure 1. X-ray diffraction patterns from the catalysts (a) RJO-137B, (b) RJO-137D, (c) RJO-137H and (d) RJO-137M.

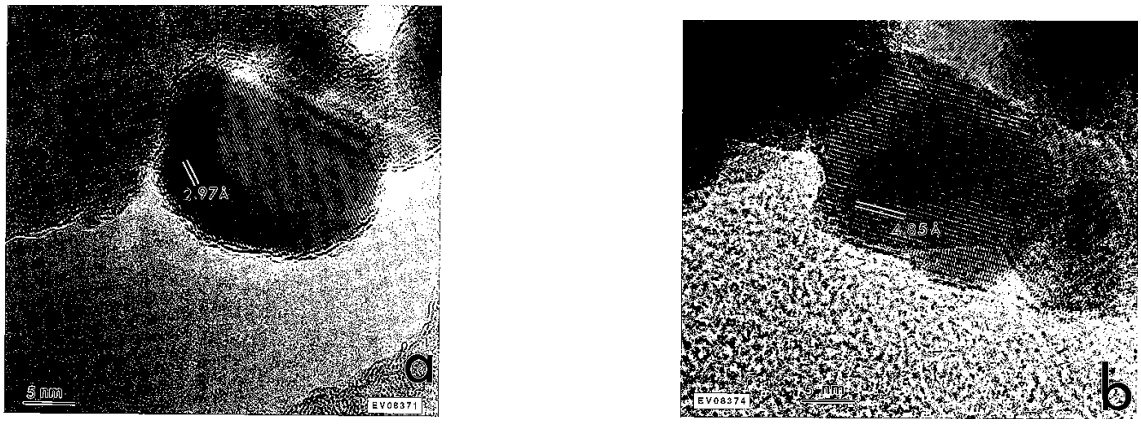


Figure 2. Lattice fringe images form 2.97 Å and 4.85 Å lattices corresponding to [220] and [111] planes of $Fe_3O_4$.

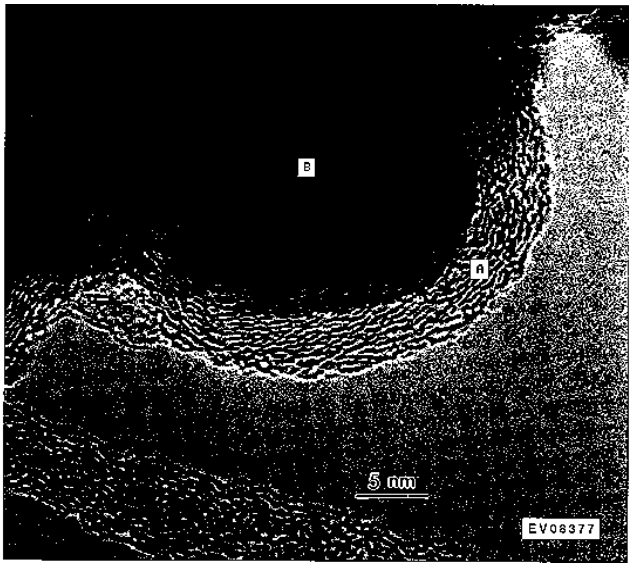


Figure 3. A $Fe_3O_4$ particle with a film of graphitic carbon. The film thickness is about 42 Å.

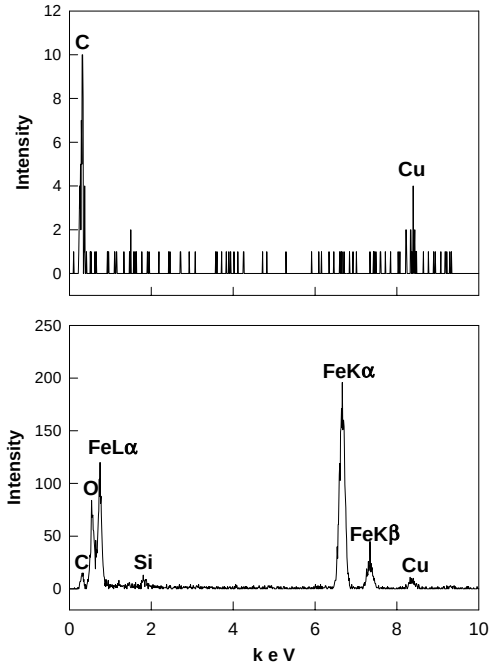


Figure 4. EDS pattern using a 1 nm probe from (a) the film and (b) the center of the particle.

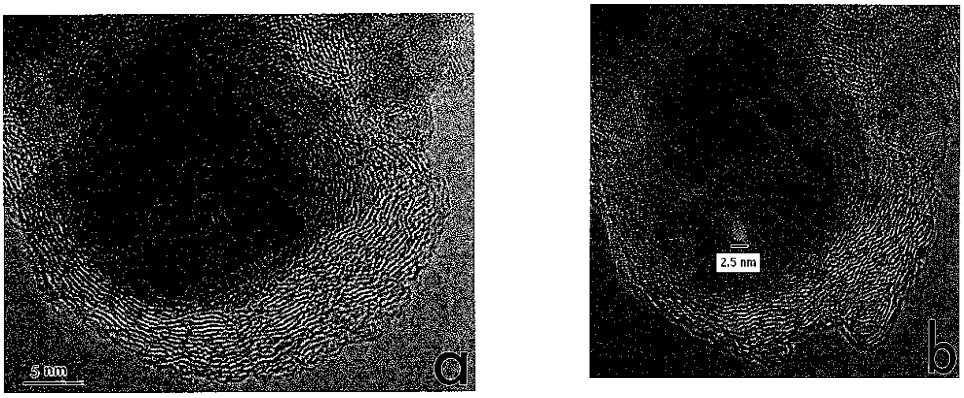


Figure 5. (a) A particle with graphitic carbon film. (b) Same particle after irradiation of 1 nm probe beam for 75 sec. Beam damage of the specimen can be seen.

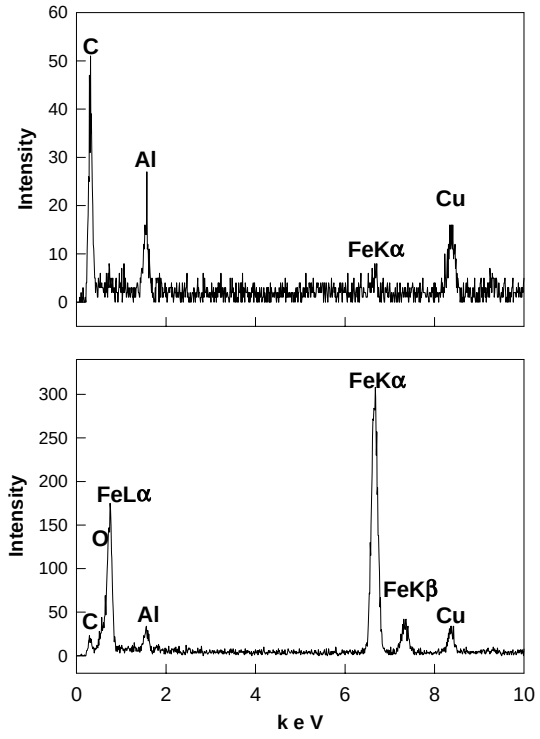


Figure 6. EDS pattern obtained from (a) the outer film and (b) the center of the particle.

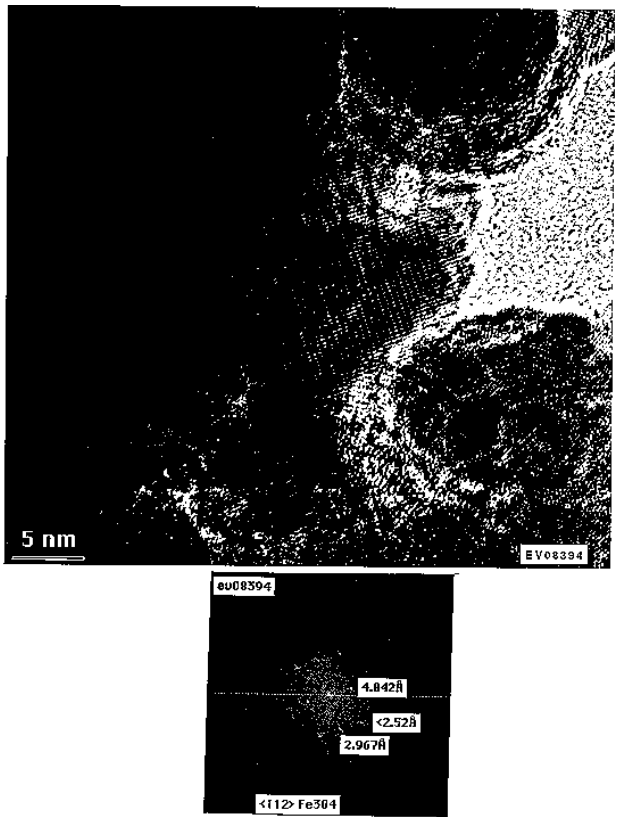


Figure 7. (a) Lattice fringe image from an $Fe_3O_4$ particle, (b) corresponding FFT pattern showing the $Fe_3O_4$ zone axis [211].

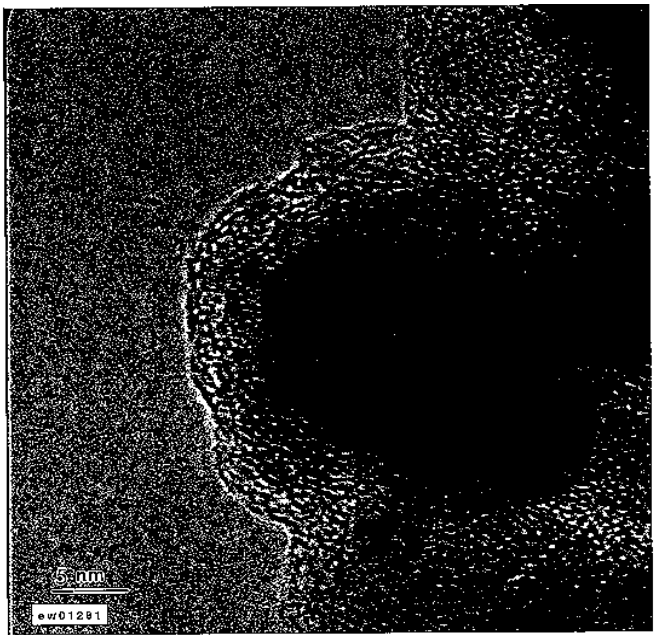


Figure 8. $Fe_3O_4$ particle with graphitic carbon film of 35 Å width.

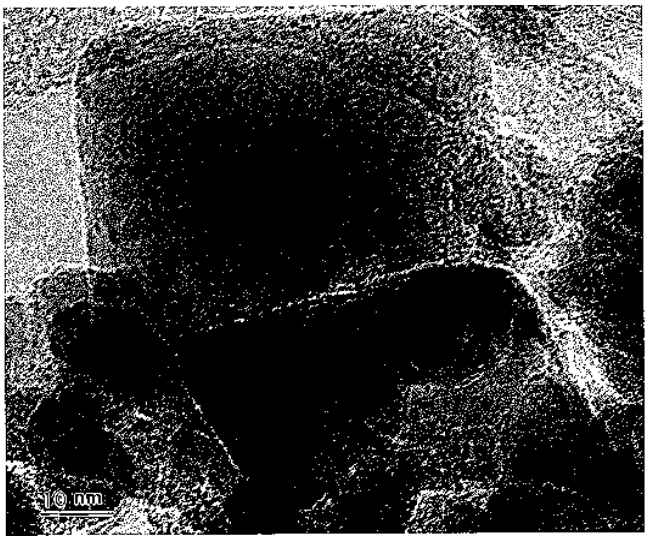


Figure 9. Typical rectangular particles from the sample RJO-137H.

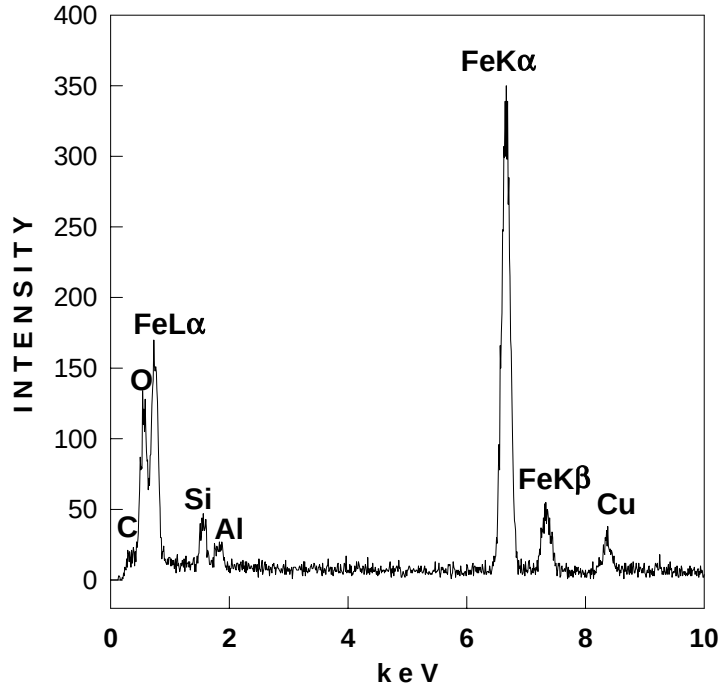


Figure 10. EDS pattern from a rectangular particle.

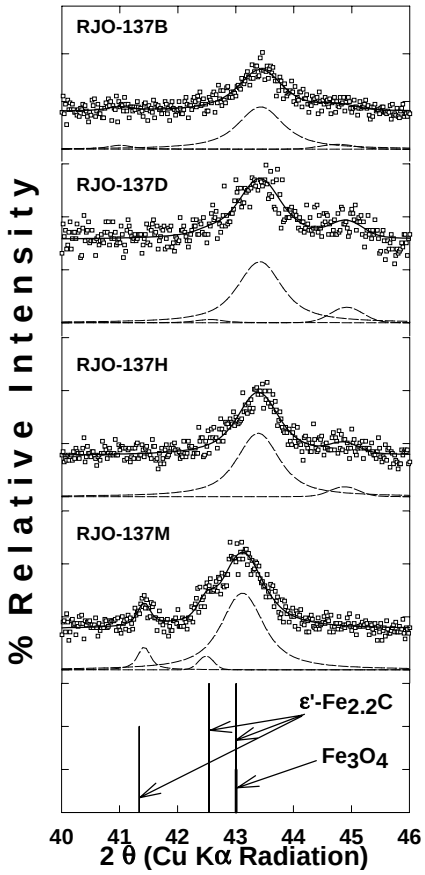


Figure 11. XRD patterns of a series of catalysts withdrawn from the CSTR reactor.

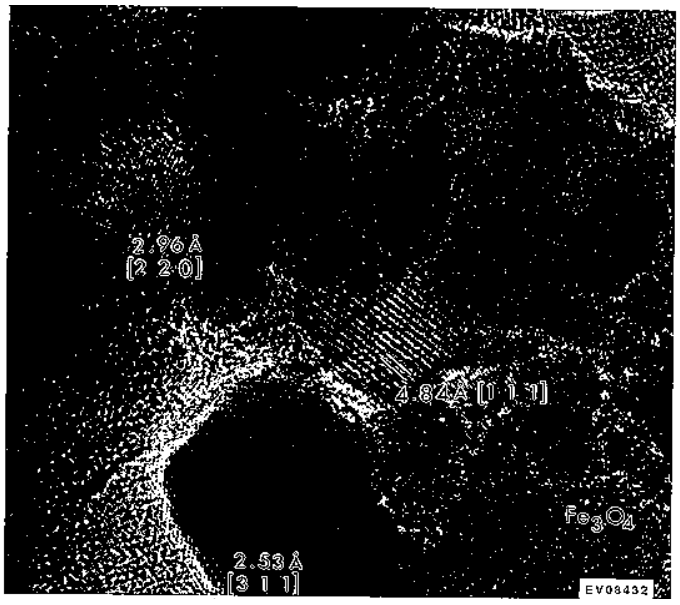


Figure 12. Scanning electron micrograph of RJO-130M showing spherical agglomerates of 30-50 µm diameter.